PAPER • **OPEN ACCESS**

Three-dimensional MHD flow in moderate change ratio orifice

To cite this article: Lorenzo Melchiorri *et al* 2022 *J. Phys.: Conf. Ser.* **2177** 012003

Journal of Physics: Conference Series 2177 (2022) 012003 doi:10.1088/1742-6596/2177/1/012003

Three-dimensional MHD flow in moderate change ratio orifice

Lorenzo Melchiorri, Alessandro Tassone, Gianfranco Caruso

DIAEE–Sapienza University of Rome, Corso Vittorio Emanuele II, 244, 00186 Roma, Italy

lorenzo.melchiorri@uniroma1.it

Abstract. In fusion reactor blanket design, liquid metals are attractive working fluids since it is possible to combine in a single fluid the functions of coolant, tritium carrier and breeder. These electrically conductive fluids flow in the presence of a strong magnetic field, inducing the appearance of Lorentz forces and magnetohydrodynamic MHD effects. Increased pressure loss, particularly in complex geometry elements, is a critical point for blanket design. The MHD flow through an orifice plate made by electroconductive walls (c = 0.01 ÷ 0.1) has been analysed in this paper using ANSYS CFX in the range Re = 108, and Ha = 0 ÷ 300. A wide recirculation region is detected after the flow exits the orifice, with potentially harmful consequences for efficient tritium removal. Large pressure loss occurs in the orifice due to conductive wall and non-negligible axial length. The 3D pressure drop term is characterized through a local resistance coefficient (k) that is found to be k ≈ 0.205 for well conducting walls (c = 0.1) and k ≈ 0.063 for poorly conducting ones (c = 0.01).

1. Introduction

In fusion reactor blankets, liquid metals are attractive due to the possibility to combine in a single fluid the functions of coolant, tritium carrier and breeder. These electrically conductive fluids interact with the intense magnetic field ($\approx 4 - 8\,T$), used to confine the plasma, causing the appearance of magnetohydrodynamic (MHD) phenomena. Increased pressure drop and flow redistribution are two effects that need to be correctly quantified to support the blanket design [1]. If the fully developed flow behavior is well understood, prediction of MHD pressure losses for developing flows in complex geometrical elements is considerably harder and far from a satisfactory theoretical explanation due to the many governing parameters involved [2]. Experiments and numerical simulations in prototypical configurations are used to estimate these losses and support the blanket design.

Sudden cross-section expansion and contraction are common hydraulic elements that exhibit complex MHD flow features like 3D currents and internal free shear layers originating from the corners [3], [4]. As such, they contribute considerably to the blanket pressure loss and, thus, an accurate estimate is of paramount importance. The most important experimental work dealing with this topic is probably the one performed by Bühler et al. [5]. Numerous simulations have been performed to characterize these components in terms of pressure loss and flow features for both insulating [6]–[9] and electrically conductive [10]–[14] rectangular ducts. A critical point is the orientation of the preferential direction for the duct expansion/contraction regarding the magnetic field, parallel variation being the most pressure loss intensive.

Considerably less studied is the simultaneous effect of a contraction followed by an expansion, as

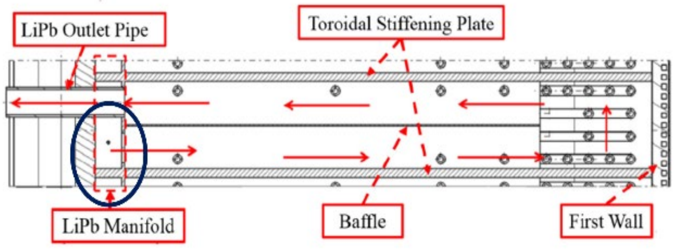

Figure 1: Breeding zone cell: radial-poloidal view, orifice position highlighted [15].

occurs whenever an orifice is met by the fluid. Only two numerical works that have addressed this topic are known to the authors. Singh and Gohil analyzed an insulating duct featuring a rectangular and triangular-shaped orifice by means of a 2D model developed using OpenFOAM; a surprising choice given the inherent 3D flow nature of the chosen geometry [16]. Tassone and Caruso have performed a more detailed study in the framework of the ITER Test Blanket Module development, using a complete 3D model to represent the MHD flow at high magnetic field intensity in a mostly one-sided sudden expansion/contraction from a rectangular orifice [17].

This paper aims to contribute to the effort of characterizing the MHD flow through a rectangular orifice. The geometry considered is a sudden cross-section variation featuring a large restriction in the direction parallel to the magnetic field (z, toroidal) and a small one perpendicular to it (y, poloidal). The main channel is a rectangular duct with electrically conductive walls ($c = 0.01 \div 0.1$). The problem is investigated for $Re = 108$, and $Ha = 0 \div 300$. The geometry is representative of the orifice connecting the manifold and breeding zone in the Water-Cooled Lithium Lead (WCLL) blanket [18] (Figure 1), whereas scaled-down magnetic field intensity is used to reduce the computational cost.

2. Problem Formulation

The MHD governing equations are obtained by the combination of the hydrodynamic set with Maxwell's one [4]. For an electrically conducting, incompressible, and viscous fluid, these equations can be written for an isothermal flow as

$$\frac{1}{N}\left(\frac{\partial}{\partial t} + \mathbf{v}\cdot\nabla\right)\mathbf{v} = -\nabla\mathbf{p} + \frac{1}{Ha^2}\nabla\mathbf{v}^2 + \mathbf{J}\times\mathbf{B} \tag{1}$$

$$\nabla\cdot\mathbf{v} = 0, \qquad \nabla\cdot\mathbf{J} = 0 \tag{2}$$

$$\mathbf{J} = -\nabla\phi + \mathbf{v}\times\mathbf{B} \tag{3}$$

Where $\mathbf{v}$, p, $\mathbf{J}$, $\mathbf{B}$ and ϕ represents velocity, pressure, current density, magnetic field, and electric potential. The variable scales are taken as described in Ref. [10]. The characteristic length scale is the duct half-width in the magnetic field direction (a). The magnetic field is assumed to be constant and aligned to the toroidal direction, $\mathbf{B} = B_0\hat{\mathbf{z}}$, thus neglecting any poloidal field contribution. Using the low magnetic Reynolds number approximation, $\mathbf{B}$ is independent by $\mathbf{v}$, and the set is closed with an additional equation obtained by combining Eqs. (2) and (3):

$$\nabla^2\phi = \nabla\cdot(\mathbf{v}\times\mathbf{B}) \tag{4}$$

The dimensionless parameter governing the flow are the Hartmann number ($Ha = a\,B_0(\sigma/\mu)0.5$), whose square is the ratio between electromagnetic and viscous forces, and the interaction parameter ($N = \sigma a B_0/\rho u_0 = Ha^2/Re$), the ratio of electromagnetic and inertial forces. The problem geometry is shown in Figure 2.

The duct is characterized by an aspect ratio γ and is bounded by uniform thickness walls (t_w). The square orifice is characterized by a toroidal (R_z) and poloidal (R_y) change ratio, as well as an axial shape factor (R_x). A uniform velocity u_0 is assumed at the inlet, which is placed at X_1 = -9a, whereas p=0 at the outlet, located at X_2 = 24a. These values are chosen to ensure a fully developed state is reached before and after the orifice. In Table 1, geometrical parameters are collected.

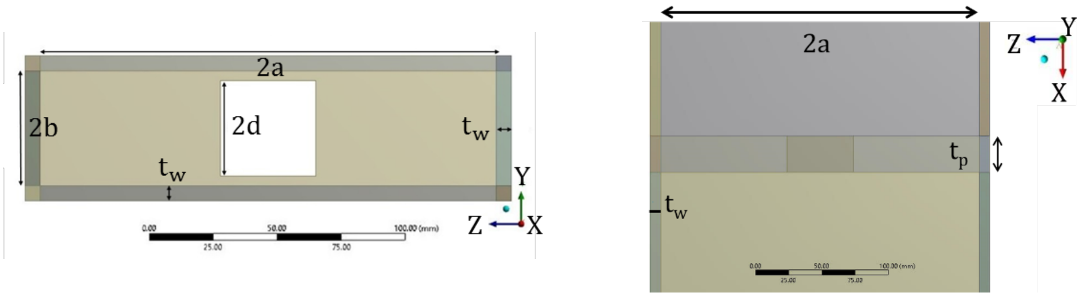

Figure 2: Problem geometry: (left) duct/orifice cross-sectional view; (right) detail of orifice, top view.

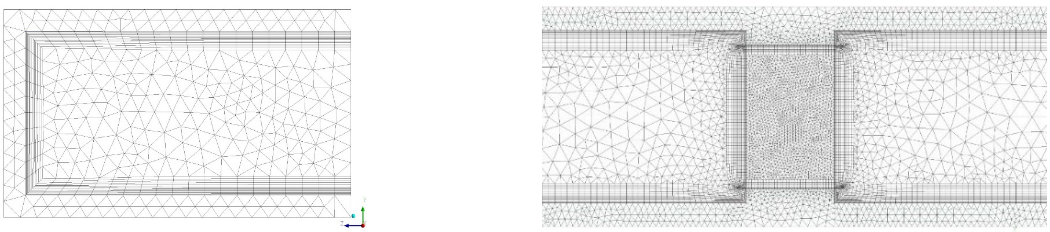

Figure 3: Computational grid: (left) duct mesh, (right) detail of orifice mesh, lateral view.

Table 1: Model geometrical parameters.

Parameter	Symbol	Value (mm)	Parameter	Symbol	Value
Duct toroidal half-length	a	120	**Duct aspect ratio**	γ	a/b = 4
Duct poloidal half-length	b	30	**Toroidal change ratio**	R_z	a/d = 4.8
Orifice half-width	d	25	**Orifice axial shape factor**	R_x	t_p /2d = 0.6
Wall thickness	t_w	8	**Poloidal change ratio**	R_y	b/d = 1.2
Plate radial thickness	t_p	30			

Since the problem features finite conductivity walls (c = 0.01 ÷ 0.1), the relative conductance ratio between wall and fluid is introduced, $c = \sigma_w t_w/(\sigma a)$, and Eq. (4) is a conjugated problem across the fluid and solid domain. At the fluid/solid interface, kinematic no-slip (**v** = 0), continuity of electric potential ($\phi = \phi_w$), and normal current ($J_n = J_{n,w}$) are the boundary conditions. On the solid external surface, the Neumann boundary condition is used ($\partial\phi/\partial n = 0$) to model the surrounding dielectric medium, as well as for inlet and outlet. The physical properties of both fluid and solid are constant. For the former, it is assumed lithium-lead at 600 K [19], for the latter σ_w is adjusted to obtain c.

3. Numerical Model

The model is solved with ANSYS CFX 18.2. For all the simulations performed, high resolution advection scheme is adopted. The convergence of the solution is controlled with residuals values of mass, velocity and electric potential conservation and monitoring solution variables (**v**, ϕ, **J**) at fixed points during the run. Calculations are stopped when the root mean square residuals are lower than 10^{-4} and the monitored variables remain constant. The flow is modelled as laminar and steady.

The model domain is discretized using an unstructured mesh composed by tetrahedrons in the core and solid structures, whereas prismatic elements are used to resolve the boundary layers, as shown in Figure 3. The grid is realized to include at least 2 elements in the Hartmann layer appearing at walls $\perp$ **B**, whose thickness is $\delta_H = O(Ha^{-1})$. The mesh axial resolution is increased approaching the orifice

Table 2: Mesh sensitivity on hydrodynamic orifice pressure drop (from Ref. [10]) versus total axial (N_X), orifice axial (N_O), and cross-sectional (N_(Y/Z)) grid resolution.

#	N_X	N_O	N_(Y/Z)	N. of elements	Δp_o (mPa)	$\Delta p_\#$ (mPa)	Error (%)
1	92	6	96 × 24	223 460		8.289	20.3
2	112	12	144 × 36	646 544		8.003	16.1
3	132	20		1 361 608	6.89	7.822	13.5
4	150	30	192 × 48	1 480 380		7.731	12.2
5	171	45		1 575 734		7.675	11.4

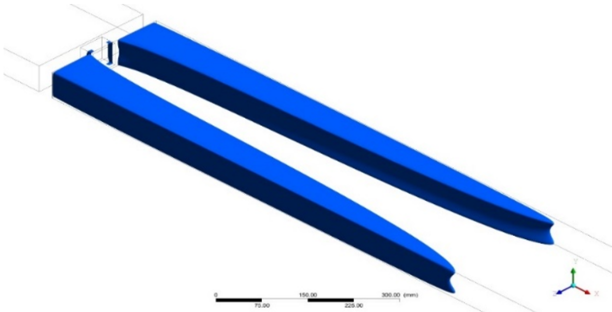

Figure 4: Negative axial velocity iso-surfaces (recirculation regions) for OHD case.

region. A mesh sensitivity study was performed comparing the hydrodynamic orifice Δp calculated by the code with the one reported by Zivkovic et al. [20] for a similar configuration. An overview of the results is presented in Table 2. The grid number 4 was selected as reference for the simulations reported in Section 4. Extensive validation of the CFX electromagnetic model has been performed in the past for pressure-driven flows in finite conductivity ducts. Details can be found in Refs. [11], [12], [15].

4. Results and Discussion

Ordinary hydrodynamic (OHD) simulations are performed to investigate basic flow features and as reference for MHD cases. It is found that contraction ratios R_z and R_y have a significantly different effect on the flow features. The poloidal contraction is relatively small, and it is not accompanied by relevant recirculation regions: the boundary layer reattachment is observed shortly after the orifice exit ($L_y \approx d$). Conversely, the toroidal contraction affects the flow features in a more dramatic fashion. Large recirculation regions are present after the orifice (Figure 4) with maximum toroidal length $L \approx 0.75\,a$. Reattachment points are located much further downstream compared with the poloidal contraction being observed about at $L_z = 40d$. Maximum velocity observed in the contraction is $u_{Max} = 1.49\ mm/s$, which still allows to treat the flow as laminar and steady since $Re_o \approx 900$. Fully developed condition is regained approximately at the axial coordinate $L_x = 72d$.

4.1. MHD Results

In Figure 5, the velocity profiles along poloidal direction within the duct (y = ±b) and inside the orifice (y = ±d) are shown. For a low magnetic field, the velocity profile in the former retains a quasi-hydrodynamic shape but, for increasing Ha, the flow separates into a slug core and jets close to the side walls. Cross-section contraction in the orifice affects the flow features more than by increasing mean velocity: M-shaped profile is observed with quicker jets and enhanced pressure losses compared with duct flow. This phenomenon is explained by the thicker Hartmann walls bounding the orifice flow, c = 6.13 versus c = 0.1. A non-null velocity gradient appears along the duct axis when the flow approaches the orifice contraction that induces an electric potential difference, as shown in Figure 6. This drives 3D currents that are not confined to the cross-section (see Figure 7). These are responsible for non-axial

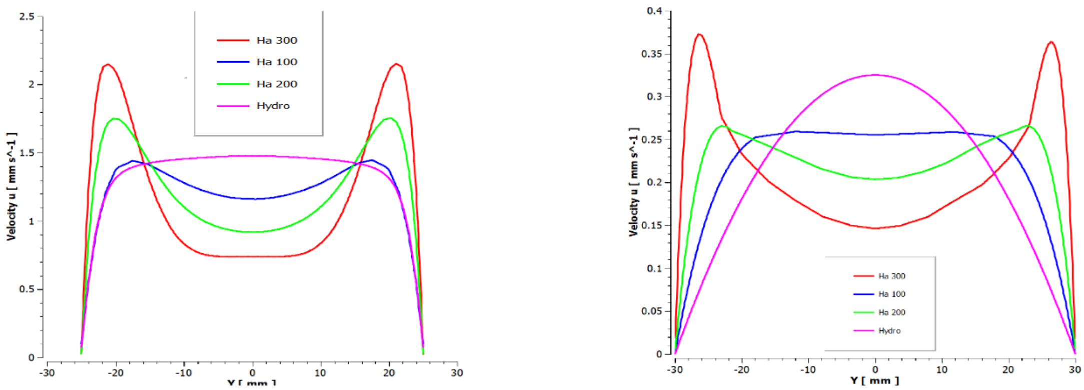

Figure 5: Velocity profile along y-direction (at midplane z = 0) for increasing Ha with c = 0.1 and OHD case: (left) at the orifice center (x=0) and fully developed flow in the duct (right).

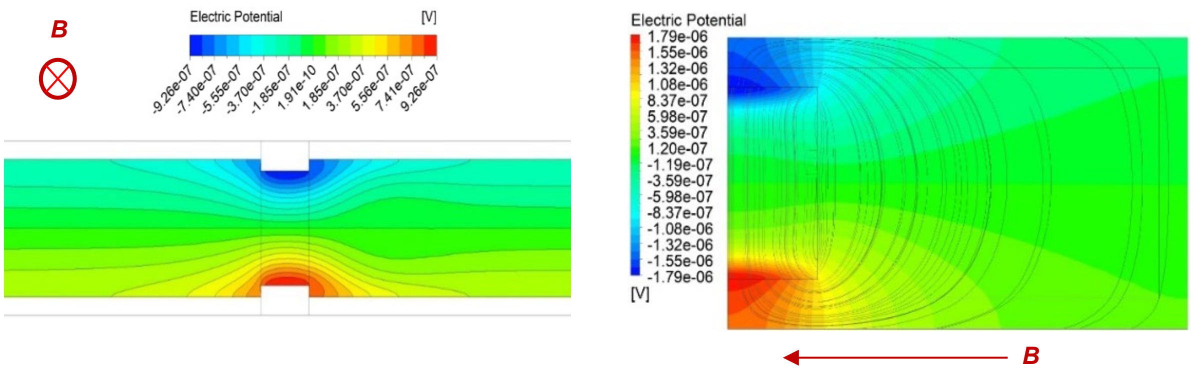

Figure 6: Electric potential contours and current density streamlines: left, z = 0 Ha = 100 c = 0.01; right, x = 0 Ha = 300 c =0.1.

Lorentz forces that causes flow redistribution and additional pressure losses. In Figure 8, it is possible to observe how the interaction between these forces, which push the fluid toward the side walls, and the flow transfer in the internal layer parallel to the magnetic field (not shown) causes core flow reversal at the duct exit. This phenomenon seems to be characteristic of the asymmetric expansion, since it is not reported by Refs. [10], [11], [17], and could lead to tritium accumulation in the manifold. It is interesting to note that a similar phenomenon was described by Rhodes et al. [8] for the sudden expansion from an insulated duct, where a pair of counter-rotating steady vortices were observed downstream of the cross-section variation. To the best of our knowledge, it is the first time that this feature is reported for electrically conductive walls. Smaller flow reversals are observed in the corners after the poloidal expansion. The recirculation region at the egress of the orifice plate appears for all the cases studied but for the lowest magnetic field intensity considered (Ha = 100). The volume of the region is found to increase with c but decreases with Ha. The flow reversal can be explained considering that jets within the orifice are quicker than the ones in the duct and are further enhanced at the orifice exit due to the effect of the axial current: these concurring phenomena cause a flow deficit in the duct central region and the formation of the recirculation. Secondary flow reversals are observed in the corners after the poloidal expansion whereas the Hartmann boundary layer does not undergo any separation. The flow regains fully developed state quicker than in the hydrodynamic simulation thanks to the stabilizing effect of the magnetic field. The orifice effect on the flow can be considered limited to an axial region $L_x = \pm 5\ d$. In Table 3, recirculation zone dimensions are collected.

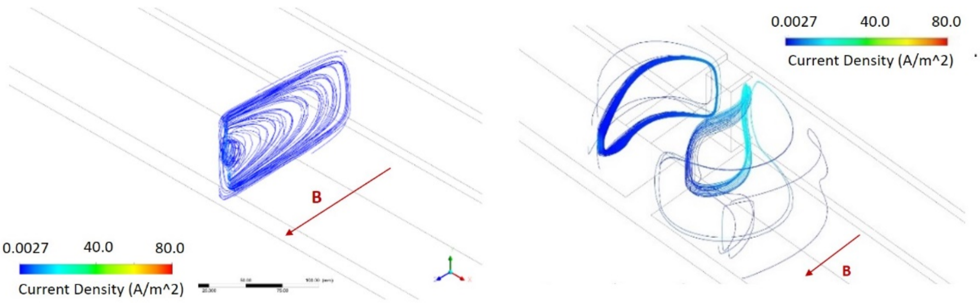

Figure 7: Current density streamlines Ha = 200 c = 0.1; straight duct (left), upstream and downstream the orifice (right).

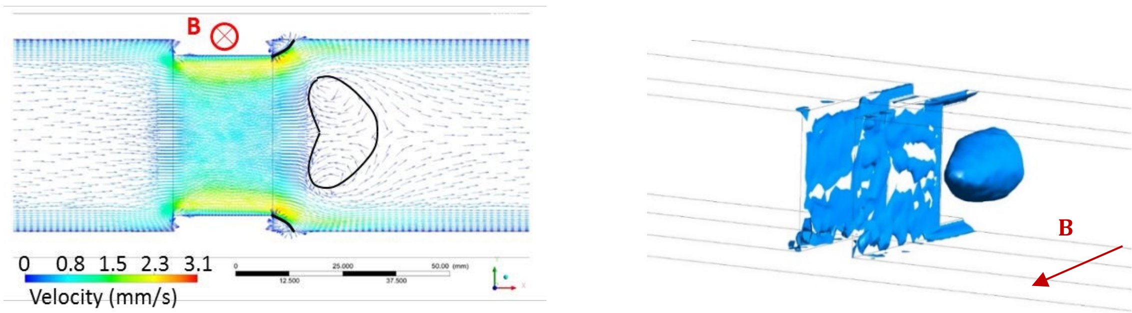

Figure 8: Left, velocity vector on the plane passing through the duct center (z=0) for Ha = 300 and c = 0.1. Flow reversals contoured in black. Right, 3D view of flow reversal for the same case.

Table 3: Downstream primary reverse flow area extension (scaled with orifice half-width d).

		Axial	Toroidal	Poloidal
Ha = 300	**c= 0.01**	0.68	2.75	0.72
	c = 0.1	0.95	4.6	1.24
Ha = 200	**c= 0.01**	0.64	1.91	0.46
	c = 0.1	0.81	3.41	0.8

4.2. Pressure Loss Analysis

If Ha $\gg$ 1, the pressure losses in an MHD flow are dominated by the Lorentz force. In Figure 9, the pressure profile for the flow through the orifice is sketched. The dashed lines represent the pressure profile for a fully developed flow in the main duct, downstream and upstream, and within the orifice region. For the former, it is computed from the area-averaged pressure gradient at the outlet ($\partial_x p_1$), whereas the latter is calculated from the area-averaged pressure gradient at the orifice center ($\partial_x p_2$). As previously noted, 2D MHD flow in the orifice features higher losses than in the duct due to a larger value of wall conductivity. A 3D pressure drop term (Δp_{3D}) is associated to the flow within the orifice due to the appearance of axial currents. It is calculated from the total pressure loss in the model: $\Delta p_{3D} = \Delta p_{tot} - 33a\partial_x p_1 - t_p \partial_x p_2$. Results are presented in Table 4.

In general, Δp_{3D} is influenced by Ha, N, c, and geometrical parameters. For constant c, increasing Ha results in a relative Δp_{3D} decrease over the total one due to a weaker dependence on B compared with 2D MHD flow, for which $\Delta p_{2D} \propto B^2$. A similar trend is observed for increasing c at constant Ha, since an increment of wall conductivity affects more the intensity of the currents closing through it rather than those which are contained within the fluid. The pressure loss can be calculated with $\Delta p_{3D} = 0.5k\sigma u_0 B_0^2 d$, where u_0 and k are the orifice hydrodynamic mean velocity and local MHD resistance coefficient. Regarding this parameter, it converges to $k \approx 0.205$ for $c = 0.1$, hinting to Δp_{3D} being determined by electromagnetic forces Ha = 200 ÷ 300, whereas inertial forces are still significant for c = 0.01 up to Ha = 300.

5. Conclusions

The 3D MHD flow in an orifice with asymmetrical sudden cross-section variation has been studied

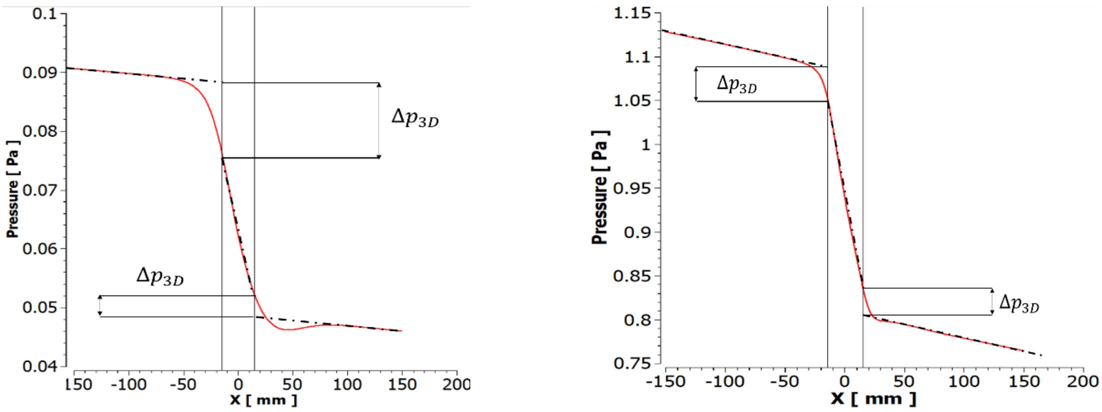

Figure 9: Pressure profiles along the duct centerline for the flow through the orifice: (left) Ha = 100 and c = 0.01, (right) Ha = 300 and c = 0.1. Vertical lines identify the orifice region. Dashed lines mark the pressure distribution for a fully developed flow in the main and orifice channel.

Table 4: 3D orifice pressure loss and MHD local resistance coefficient.

	c=0.01			c=0.1		
Ha	**100**	**200**	**300**	**100**	**200**	**300**
Δp(Pa)	0.04821	0.1279	0.2374	0.1057	0.3727	1.3888
Δp_{3D}(Pa)	0.00784	0.0107	0.0201	0.0134	0.0291	0.0669
k	0.221262	0.075278	0.062891	0.378225	0.204729	0.209324
$\Delta p_{3D}/\Delta p$	16.26%	8.36%	8.48 %	12.72%	7.8 %	4.82 %

using the code ANSYS CFX in the range Ha = 0 ÷ 300 and c = 0.01 ÷ 0.1. The geometry considered is representative of the perforated plate connecting the manifold and breeding zone in the WCLL [15]. The flow main features are described with the most interesting one being the appearance of a wide recirculation region at the exit. The 3D pressure loss for the flow through the orifice can be estimated with $k \approx 0.205$ for $c = 0.1$ and $k \approx 0.063$ for $c = 0.01$.

Further work is required to complete the characterization of the MHD flow through a rectangular orifice. It would be desirable to perform simulation closer to blanket conditions, i.e. featuring Ha ≈ 10^4. An important point that has so far been neglected in the literature is the effect of a skewed magnetic field on the 3D loss. The effect of the orifice shape and axial length should also be investigated and its role in the onset of recirculation regions downstream of it.

Acknowledgments This work has been carried out within the framework of the EUROfusion Consortium and has received funding from the Euratom research and training programme 2014-2018 and 2019-2020 under grant agreement No 633053. The views and opinions expressed herein do not necessarily reflect those of the European Commission.

References

[1] S. Smolentsev, R. Moreau, L. Bühler, and C. Mistrangelo, "MHD thermofluid issues of liquid-metal blankets: Phenomena and advances," *Fusion Eng. Des.*, vol. 85, no. 7–9, pp. 1196–1205, 2010, doi: 10.1016/j.fusengdes.2010.02.038.
[2] S. Smolentsev, "Physical Background, Computations and Practical Issues of the Magnetohydrodynamic Pressure Drop in a Fusion Liquid Metal Blanket," *Fluids*, vol. 6, no. 3, p. 110, 2021, doi: 10.3390/fluids6030110.
[3] J. C. R. Hunt and S. Leibovich, "Magnetohydrodynamic flow in channels of variable cross-section with strong transverse magnetic fields," *J. Fluid Mech.*, vol. 28, no. 2, pp. 241–260, 1967, doi: 10.1017/S0022112067002046.
[4] U. Muller and L. Bhuler, *Magnetofluiddynamics in Channels and Containers*. 1999.
[5] L. Bühler, S. Horanyi, and E. Arbogast, "Experimental investigation of liquid-metal flows through a sudden expansion at fusion-relevant Hartmann numbers," *Fusion Eng. Des.*, vol. 82, no. 15–24, pp. 2239–2245, 2007, doi: 10.1016/j.fusengdes.2007.02.029.
[6] J. Feng, Q. He, H. Chen, and M. Ye, "Numerical Investigation of magnetohydrodynamic flow through Sudden expansion pipes in Liquid Metal Blankets," *Fusion Eng. Des.*, vol. 109–111, pp. 1360–1364, 2016, doi: 10.1016/j.fusengdes.2015.12.023.
[7] H. Kumamaru, "Numerical analyses on liquid-metal magnetohydrodynamic flow in sudden channel contraction," *J. Nucl. Sci. Technol.*, vol. 54, no. 12, pp. 1300–1309, 2017, doi: 10.1080/00223131.2017.1365021.
[8] T. J. Rhodes, S. Smolentsev, and M. Abdou, "Magnetohydrodynamic pressure drop and flow balancing of liquid metal flow in a prototypic fusion blanket manifold," *Phys. Fluids*, vol. 30, no. 5, 2018, doi: 10.1063/1.5026404.
[9] T. Rhodes and S. Smolentsev, "Pressure drop in a prototypical 3D magnetohydrodynamic flow across contraction of a fusion blanket manifold," *J. Nucl. Sci. Technol.*, vol. 00, no. 00, pp. 1–10, 2021, doi: 10.1080/00223131.2021.1892550.
[10] C. Mistrangelo and L. Bühler, "Numerical investigation of liquid metal flows in rectangular sudden expansions," *Fusion Eng. Des.*, vol. 82, no. 15–24, pp. 2176–2182, 2007, doi: 10.1016/j.fusengdes.2007.04.014.
[11] C. N. Kim, "Liquid metal magnetohydrodynamic flows in an electrically conducting rectangular duct with sudden expansion," *Comput. Fluids*, vol. 89, pp. 232–241, 2014, doi: 10.1016/j.compfluid.2013.11.002.
[12] C. N. Kim, "A liquid metal magnetohydrodynamic duct flow with sudden contraction in a direction perpendicular to a magnetic field," *Comput. Fluids*, vol. 108, no. 1000, pp. 156–167, 2015, doi: 10.1016/j.compfluid.2014.12.001.
[13] L. Bühler, "A parametric study of 3D MHD flows in expansions of rectangular ducts," *Fusion Sci. Technol.*, vol. 52, no. 3, pp. 595–602, 2007, doi: 10.13182/FST07-A1553.
[14] X. Xiao and C. N. Kim, "Numerical simulations of MHD flows in a conduit that contracts in the magnetic field direction," *Fusion Eng. Des.*, vol. 160, no. July, p. 111990, 2020, doi: 10.1016/j.fusengdes.2020.111990.
[15] A. Tassone, G. Caruso, A. Del Nevo, and I. Di Piazza, "CFD simulation of the magnetohydrodynamic flow inside the WCLL breeding blanket module," *Fusion Eng. Des.*, vol. 124, pp. 705–709, 2017, doi: 10.1016/j.fusengdes.2017.05.098.
[16] R. J. Singh and T. B. Gohil, "Influence of the presence of the Lorentz force and its direction on the suppression of secondary flow in two different orifices: A numerical study using OpenFOAM," *J. Appl. Fluid Mech.*, vol. 12, no. 3, pp. 751–762, 2019, doi: 10.29252/JAFM.12.03.29242.
[17] A. Tassone and G. Caruso, "Computational MHD analyses in support of the design of the WCLL TBM breeding zone," *Fusion Eng. Des.*, vol. 170, no. February, p. 112535, 2021, doi: 10.1016/j.fusengdes.2021.112535.
[18] A. Del Nevo *et al.*, "Recent progress in developing a feasible and integrated conceptual design

of the WCLL BB in EUROfusion project," *Fusion Eng. Des.*, vol. 146, no. March, pp. 1805–1809, 2019, doi: 10.1016/j.fusengdes.2019.03.040.

[19] D. Martelli, A. Venturini, and M. Utili, "Literature review of lead-lithium thermophysical properties," *Fusion Eng. Des.*, vol. 138, no. November 2018, pp. 183–195, 2019, doi: 10.1016/j.fusengdes.2018.11.028.

[20] V. Zivkovic, P. Zerna, Z. T. Alwahabi, and M. J. Biggs, "A pressure drop correlation for low Reynolds number Newtonian flows through a rectangular orifice in a similarly shaped micro-channel," *Chem. Eng. Res. Des.*, vol. 91, no. 1, pp. 1–6, 2013, doi: 10.1016/j.cherd.2012.05.022.